Lamellar grating optimization for miniaturized fourier transform spectrometers

Onur Ferhanoglu[1,3], Hüseyin R. Seren[1,3]*, Stephan Lüttjohann[2] and Hakan Urey[1]

[1]*Department of Electrical Engineering, Koç University, Sarıyer, Istanbul 34450, Turkey*
[2]*Bruker Optics, Ettlingen, Germany*
[3]*These authors contributed equally to this work.*
**hurey@ku.edu.tr*

Abstract: Microfabricated Lamellar grating interferometers (LGI) require fewer components compared to Michelson interferotemeters and offer compact and broadband Fourier transform spectrometers (FTS) with good spectral resolution, high speed and high efficiency. This study presents the fundamental equations that govern the performance and limitations of LGI based FTS systems. Simulations and experiments were conducted to demonstrate and explain the periodic nature of the interferogram envelope due to Talbot image formation. Simulations reveal that the grating period should be chosen large enough to avoid Talbot phase reversal at the expense of mixing of the diffraction orders at the detector. Optimal LGI grating period selection depends on a number of system parameters and requires compromises in spectral resolution and signal-to-bias ratio (SBR) of the interferogram within the spectral range of interest. New analytical equations are derived for spectral resolution and SBR of LGI based FTS systems.

©2009 Optical Society of America

OCIS codes: (050.1950) Diffraction gratings; (070.6760) Talbot and self-imaging effects; (070.7345) Wave propagation; (300.6290) Spectrometers.

References and links

1. V. Saptari, "Fourier-Transform Spectroscopy Instrumentation Engineering", SPIE International Society for Optical Engineering, 2003.
2. T. Sandner, C. Drabe, H. Schenk, A. Kenda, and W. Scherf, "Translatory MEMS actuators for optical path length modulation in miniaturized Fourier-transform infrared spectrometers," MEMS MOEMS **7**(2), 021006 (2008).
3. J. Strong, and G. A. Vanasse, "Lamellar grating far-infrared interferometer," J. Opt. Soc. Am. **50**(2 Issue 2), 113 (1960).
4. O. Manzardo, R. Michaely, F. Schädelin, W. Noell, T. Overstolz, N. De Rooij, and H. P. Herzig, "Miniature lamellar grating interferometer based on silicon technology," Opt. Lett. **29**(13), 1437–1439 (2004).
5. C. Ataman, H. Urey, and A. Wolter, "MEMS-based Fourier Transform Spectrometer," J. Micromechanics and Microengineering **16**, 2516–2523 (2006).
6. J. W. Goodman, Introduction to Fourier Optics, Roberts & Company Publishers, 2005.
7. C. Ataman, H. Urey, "Compact Fourier Transform Spectrometers using FR4 Platform" SNA: A. Physical, A 151 (2009) 9–16.
8. R. T. Hall, D. Vrabec, and J. M. Dowling, "A High-Resolution, Far Infrared Double-Beam Lamellar Grating Interferometer," Appl. Opt. **5**(7), (1966).
9. R. L. Henry, and D. B. Tanner, "A Lamellar Grating Interferometer for the Far-Infrared," Infrared Phys. **19**(2), 163–174 (1979).
10. F. Lee, G. Zhou, H. Yu, and F. S. Chau, "A MEMS-based resonant-scanning lamellar grating Fourier transform micro-spectrometer with laser reference system," Sens. Actuators A Phys. **149**(2), 221–228 (2009).

1. Introduction

Fourier transform spectrometry (FTS) is an established method that finds use in a variety of applications such as chemical substance detection and analysis, quality control, mining, or bomb detection. FTS is performed by measuring an interference signal which has the whole information about the spectrum of the light. Conventional FTS devices use a Michelson interferometer that is composed of a beam splitter, a stationary mirror, and a moving mirror which occupy a significant amount of space [1,2]. However, FTS can also be built in a more

#115556 - $15.00 USD Received 14 Aug 2009; revised 23 Oct 2009; accepted 1 Nov 2009; published 6 Nov 2009
(C) 2009 OSA

compact manner using a lamellar grating interferometer (LGI) that utilizes a movable diffraction grating and operates in the zeroth order [3–5]. Even though the concept of LGI is known for several decades, it became practical only after the advancements in the microfabrication and Micro-electro-mechanical systems (MEMS) technologies. MEMS technology enables fabrication of very precise diffraction gratings that can move at high-speed and in a pure translation mode with simple actuation and control methods. A study regarding the limitations of LGI and optimization was missing.

This study is carried out under MEMFIS project within the EU 7th framework program which aims to build an ultrasmall mid-wave IR (MWIR) spectrometer working in the 2.5um-16um range. Figure 1(a) illustrates the basic FTS layout using a LGI. In this configuration, an infrared (IR) source is collimated with a parabolic IR mirror. The incoming beam is reflected partly from the fixed grating fingers and partly from the moving grating fingers. The two reflected beams interfere and create an interferogram at the detector in response to the changing optical path difference (OPD) between the grating fingers. The light spectrum can be computed by recording the 0th diffraction order intensity and computing its Fourier transform with OPD as the integration variable. When a sample is placed at the illustrated sample plane, the transmittance properties of the sample can be observed when compared with the source spectrum without the sample. There are other well known FTS configurations that allow recording of the reflectance and absorbance spectrum of the sample. The key advantages of the LGI configuration compared to the Michelson configuration are the elimination of the beam splitter and reference mirror, which make the system more robust, more compact and lower cost. Note that all the optics in Fig. 1 are reflective, therefore the spectral range of operation can be very broad and limited by the detector.

Our group previously demonstrated MEMS based LGI with 53um deflection operated at 1KHz [Fig. 1(b)], which can read a spectrum in ~1msec [5]. The design is based on electrostatic actuation of comb fingers to obtain a pure translatory motion that is necessary to create the interference. Besides providing comb-type electrostatic actuation, the aluminum coated comb fingers also function as reflectors for the lamellar grating where an optical path difference is created between the movable and fixed fingers. The next generation design being fabricated has a predicted peak-to-peak OPD >1mm and should achieve $<10\text{cm}^{-1}$ spectral resolution.

Decreasing the size of a complete FTIR system without any performance degradation requires optimization at many levels. This study particularly focuses on the optical design aspects and optimization of the grating period size in order to achieve best efficiency, spectral resolution, and signal-to-bias ratio at the detector. The relationship between the Talbot image distance and spectral resolution is investigated for the first time and a new fundamental equation for spectral resolution of LGI systems is derived.

#115556 - $15.00 USD Received 14 Aug 2009; revised 23 Oct 2009; accepted 1 Nov 2009; published 6 Nov 2009
(C) 2009 OSA

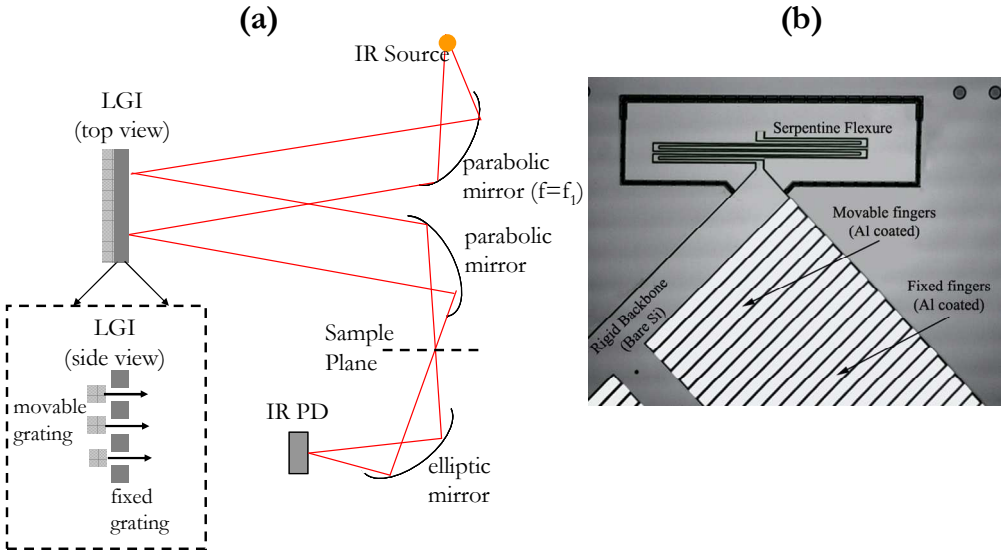


Fig. 1. (a) Cartoon drawing of an LGI based FTS system illustrating IR source, parabolic and elliptic mirrors, LGI, sample plane and IR photodetector. Side view illustrates the moving and fixed fingers (b) Microscope picture of a MEMS LGI fabricated on Silicon wafer. Each grating finger is 1.2 mm long, 70um wide with 5um gap in between [5].

2. LGI theory

Four basic limitations of the Fourier Transform Spectrometers are revisited in this section. First two limitations are related to the spectral resolution set by the optical path difference in the interferometer arms and the divergence of the source, which are applicable to both Michelson and LGI based FTS. Additional limitations that apply to LGI spectrometers only are based on the mixing of diffracted orders and the Talbot effect that is explained in detail throughout the section.

The spectral operation range of an FTS is defined as [λ_{min} - λ_{max}] and in terms of the wavenumber $k = 1/\lambda$ as [$k_{max} - k_{min}$]. The spectral resolution of the FTS depends on the distance that the moving part travels, $\pm d$, and how well the source is collimated. Assuming a point source which can be collimated perfectly, the spectral resolution is expressed with the well known equation [1]

$$\Delta k = \frac{1}{OPD} = \frac{1}{2d} \tag{1}$$

where Δk is the spectral resolution, OPD stands for optical path difference between the two parts of the interferometer, and $\boldsymbol{d}$ is the maximum deflection of the moving part of the LGI. The half divergence angle, θ_d, is a measure of how well the source is collimated, which is expressed by the size of the source (D_s) or source aperture and the focal length of the first collimating mirror (f_1):

$$\theta_d = \tan(D_s / 2f_1) \tag{2}$$

After the collimating mirror, rays travel in an unparallel fashion due to the divergence effect. Assuming a monochromatic source, two extreme rays that travel within the LGI experience different optical path difference, which can be expressed as:

$$\Delta OPD = \left| 2d(1 - \frac{1}{\cos\theta_d}) \right| \tag{3}$$

#115556 - $15.00 USD Received 14 Aug 2009; revised 23 Oct 2009; accepted 1 Nov 2009; published 6 Nov 2009
(C) 2009 OSA

A destructive interference occurs once the OPD difference is half the wavelength. Limiting OPD difference to half wavelength, and using small angle approximation such that $\cos(\theta_d) = 1 - \theta_d^2/2$ brings the following criteria to the half divergence angle in order to achieve the spectral resolution depicted by Eq. (1) [1]:

$$\theta_d \le \sqrt{\frac{\lambda_{\min}}{2d}} = \sqrt{\frac{\Delta k}{k_{\max}}} \tag{4}$$

Equation (1) and Eq. (4) apply to all interferometric Fourier Transform Spectrometers. There are other criteria that apply to only LGI spectrometers, which are based on the formation of diffraction orders. Diffraction orders are observed at integer multiples of the angle: λ/Λ where Λ is the grating period. The separation of the 0th and 1st diffraction orders for a finite source size is assured under the following condition:

$$\sin(2\theta_d) \le \lambda_{\min} / \Lambda \tag{5}$$

The main focus of this study is to bring forward and demonstrate the main resolution determining factor in LGI spectrometers, which is based on the Talbot effect [6]. The following paragraphs explain the Talbot effect and its implications on the spatial and the spectral resolution in detail:

Illumination of a periodic pattern (square-wave amplitude grating in this case) results in approximate images (Talbot images) of the grating at integer multiple of the distance [6]:

$$T = 2\Lambda^2 / \lambda \tag{6}$$

Phase reversed images appear in between two consecutive Talbot images. Figure 2(a) and Fig. 2(b) illustrate the wave pattern created after a collimated beam passes through a grating. Figure 2(a) shows the result of a vector diffraction analysis performed with COMSOL FEM software, where polarization and grating thickness effects are taken into account. The top of the grating is coated with aluminum and reflects the incident radiation. Reflection and transmission through silicon side walls of the LGI structure are also taken into account. Figure 2(b) shows the result given by the scalar diffraction calculations performed in Matlab. The results of the two analyses agree well and predict the Talbot distances accurately, which verifies the validity of our diffraction code that will be used throughout this study.

Talbot images and phase reversal can be clearly observed at the highlighted distances. Talbot phase reversal need to be avoided since nearly all the energy transmitted from the top reflector escapes between the fingers of the bottom reflector. Since little energy is reflected back from the bottom reflector, interference and the fringe contrast reduces nearly to zero. The first Talbot phase reversal appear at ½ of the Talbot distance, which effectively set the limit of the maximum usable OPD for the LGI. The same phase reversal effect is observed when a movable mirror is placed behind a fixed grating, where the phase reversed Talbot image of the returning light is blocked by the fingers of the fixed grating when the deflection is equal to ¼ of the Talbot period.

#115556 - $15.00 USD Received 14 Aug 2009; revised 23 Oct 2009; accepted 1 Nov 2009; published 6 Nov 2009
(C) 2009 OSA

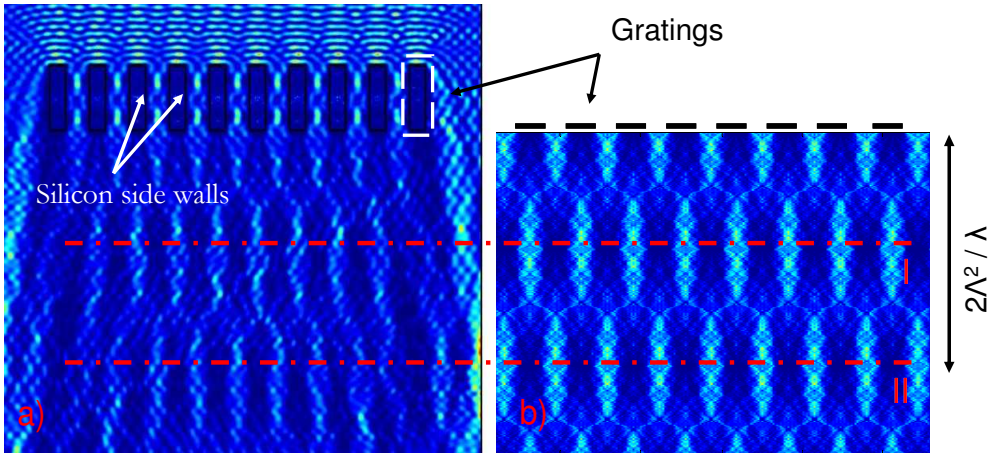


Fig. 2. Intensity pattern of Talbot (plane II) and phase reversed Talbot (plane I) images created when an amplitude grating is illuminated from top with a plane wave (only fixed grating is shown): (a) COMSOL FEM simulation tool results (b) results of our wave propagation code using scalar diffraction theory.

Talbot phase reversal can be avoided by adjusting the maximum displacement to be $d <$ T/2, which brings a new restriction to the grating period, such that:

$$\Lambda > \sqrt{\lambda_{\max} d} = \sqrt{\frac{\lambda_{\max}}{2\Delta k}} \tag{7}$$

3. FTS design case study

After the selection of the desired resolution and spectral band of operation, it is possible to calculate the maximum displacement; the maximum allowed divergence, the grating period to ensure adequate order separation while avoiding the Talbot phase reversal based on the 4 criteria given above. Assuming a desired resolution of $\Delta k = 10$ cm^{-1} and a spectrum of interest in the Mid-Wave Infrared (MWIR) λ = [2.5um - 16um], or k = [625cm^{-1} - 4000cm^{-1}], the following requirements can be derived:

- d = 500 um, based on Eq. (1)
- $\theta_d < 2.5°$, based on Eq. (4),
- $\Lambda < 25$ um, based on Eq. (5), to ensure order separation,
- $\Lambda > 90$ um, based on Eq. (7), to avoid Talbot phase reversal.

Note that using the system specifications and the fundamental equations, there are conflicting requirements on the grating period. Therefore, an optimization and compromise in system performance is required, which is the main focus of the next section.

4. Numerical simulations

4.1 Algorithm and interferogram results

Scalar diffraction theory is widely used in analyzing diffractive optical elements. Fresnel propagation codes based on scalar diffraction theory [6] were developed in MATLAB to investigate the effects of a lamellar grating structure on the spectrum measurements. Simulated model is illustrated in Fig. 3. For the MWIR wavelength range (2.5um – 16 um), the grating period in the range 50um-150um is well above the wavelength, where scalar diffraction theory provides accurate results with high computation speed.

#115556 - $15.00 USD Received 14 Aug 2009; revised 23 Oct 2009; accepted 1 Nov 2009; published 6 Nov 2009
(C) 2009 OSA

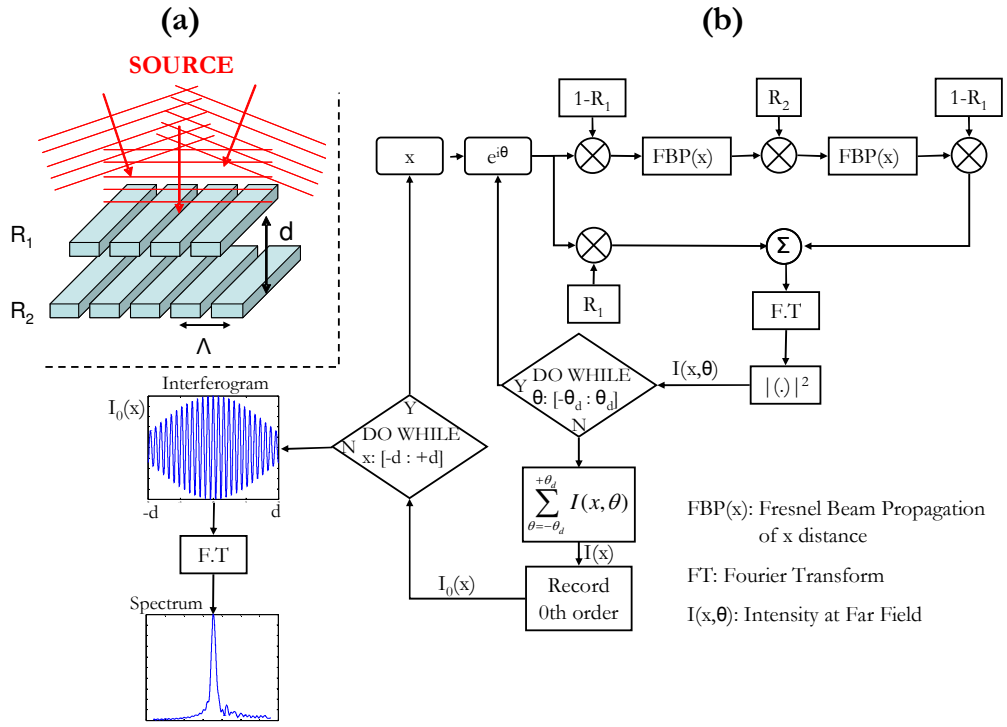


Fig. 3. (a) Lamellar grating interferometer with grating period grating deflection d, and top and bottom reflector reflectivities of R_1 and R_2; (b) diffraction calculation algorithm used for the numerical simulations.

The source is modeled as the sum of plane waves with different incidence angles to account for the divergence. The incoming wave is multiplied by an amplitude grating function (movable grating) and propagated for a distance of x. Once the transmitted wave reaches the fixed grating, the diffracted pattern is multiplied by the amplitude function of the fixed grating and the reflected beam is propagated once again a distance of x. Finally the resultant diffracted pattern is multiplied by the amplitude transmittance function of the movable grating and added with the initially reflected beam to form the reflected wave pattern. The detector intensity is then calculated after a Fraunhofer propagation, which is essentially a Fourier transformation followed by integration of the beam energy within the detector window. The procedure is repeated for all incidence angles in the range $[-\theta_d - \theta_d]$, which are added together in incoherent (i.e., intensity) basis, and for all deflections in the range $x = [-d - + d]$ to form the interferogram, which is a function of interference with respect to deflection x. The final spectrum is the modulus square of the Fourier transform of the interferogram.

For a non diverging source, constructive interference occurs at $d = n\lambda/2$ for 0th order diffracted light [Fig. 4(a)] and $d = \lambda/4 + n\lambda/2$ for the 1st order diffracted light [Fig. 4(b)] where n is any integer. Divergence of the source results in a shift on the order locations as illustrated in Fig. 4(c) for an intermediate point: $d = k\lambda/2 + \lambda/8$. The light is collected through an integration window that is tailored to include all 0th orders for the calculated half divergence angle of 2.5°. Once all 0th orders are collected, some of the 1st orders are also included within the integration window, lowering the light efficiency and fringe contrast. Effect of mixing of the orders and size of integration window on spectral resolution will be discussed further.

#115556 - $15.00 USD Received 14 Aug 2009; revised 23 Oct 2009; accepted 1 Nov 2009; published 6 Nov 2009
(C) 2009 OSA

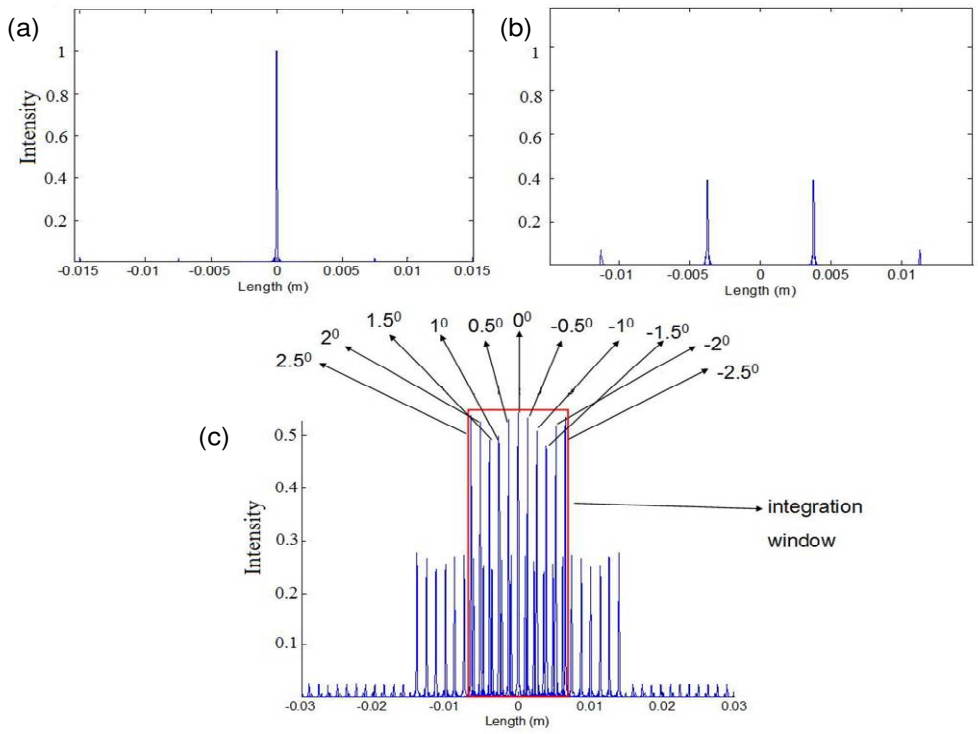


Fig. 4. Far field (observed 15 cm away from LGI for λ = 2.5 um, Λ = 100 um) pattern of a) d = k.λ/2 b) d = λ/4 + k.λ/2 c) = k.λ/2 + λ/8 for all angles between −2.5 and + 2.5 degrees with 0.5 degree intervals. Integration window is illustrated in red.

The source is assumed to be spatially incoherent, therefore the interferogram is recorded by summing the total intensity within the integration window versus displacement of the movable finger. The interferogram signal is of the form

$$I(x) = \left[B + S\cos(\frac{4\pi}{\lambda_0} x) \right].E(x) \tag{8}$$

where *E(x)* is a slowly varying envelope function effected by all the system parameters and will be discussed later. Amplitude of DC components is taken as bias and the amplitude of spectral component at excitation wavelength λ_0 is taken as the signal. Signal to Bias ratio (SBR) can be represented as

$$SBR = \frac{S}{B} \tag{9}$$

Figure 5 and Fig. 6 illustrate examples of interferograms and their spectrum for different grating periods and divergence angles. The wavelengths of interest are chosen to be the border wavelengths of MWIR region, 2.5 and 16 um respectively. Spectral resolution is then computed by calculating the main-lobe-width of a best fit *sinc* function centered on λ_o.

#115556 - $15.00 USD Received 14 Aug 2009; revised 23 Oct 2009; accepted 1 Nov 2009; published 6 Nov 2009
(C) 2009 OSA

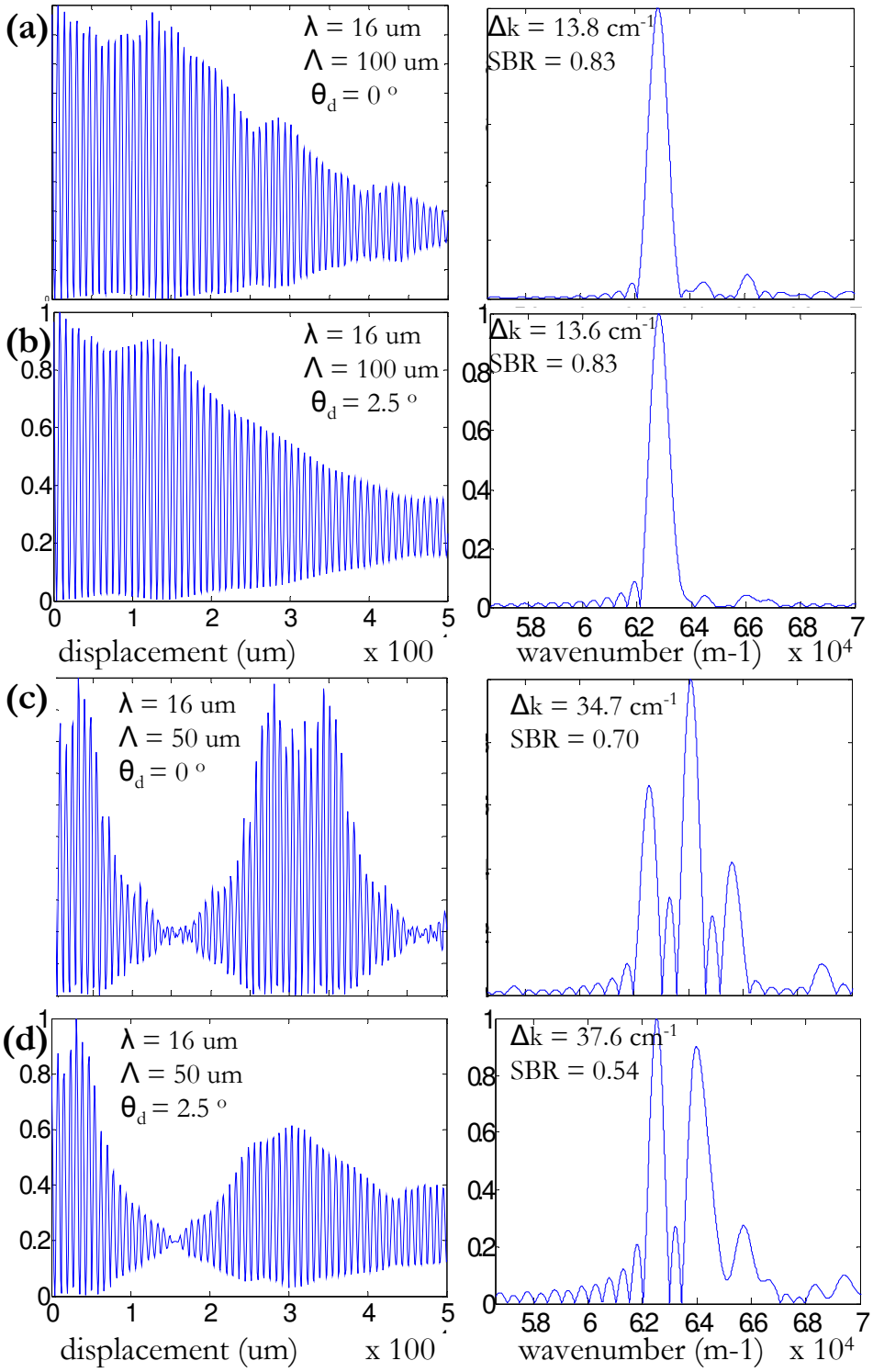


Fig. 5. Interferograms and their spectrum for 16 um illumination wavelength, Λ = 50, 100 um and $\theta_d = 0°$ and $\theta_d = 2.5°$. All plots in the same column have the same scale.

#115556 - $15.00 USD Received 14 Aug 2009; revised 23 Oct 2009; accepted 1 Nov 2009; published 6 Nov 2009
(C) 2009 OSA

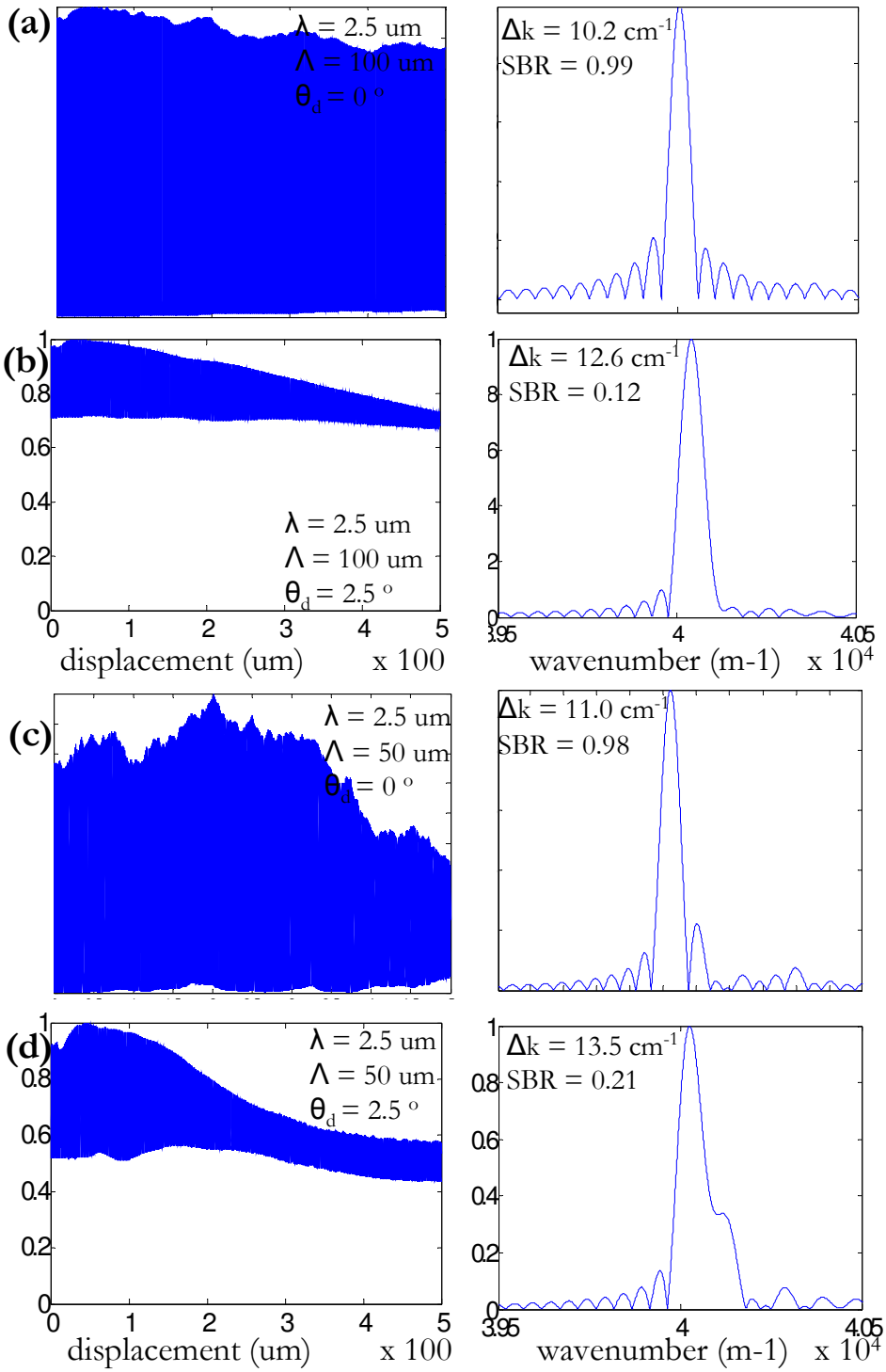


Fig. 6. Interferograms and their spectrum for 16 um illumination wavelength, Λ = 50, 100 um and $\theta_d = 0°$ and $\theta_d = 2.5°$. All plots in the same column have the same scale..

#115556 - $15.00 USD Received 14 Aug 2009; revised 23 Oct 2009; accepted 1 Nov 2009; published 6 Nov 2009
(C) 2009 OSA

Figure 5 illustrates that, for λ = 16um, since the diffraction order angles are large, the half divergence angle of 2.5° doesn't effect the spectral resolution performance. However, the effects of Talbot phase reversal are clearly seen for λ = 16 um and Λ = 50 um when d = T/2 = 156 um which is the exact location of the dip in the interferogram. The second dip takes place at 3T/2 = 469 um, exactly one Talbot period after the first dip. For Fig. 5(d), the divergence of the source prevents the fringe contrast to totally vanish, nevertheless the dip is still observable and the resultant spectral peak is multi-lobed and broadened.

In Fig. 6, λ is set to 2.5um and the effects of divergence angle on the SBR is clearly observed due to the mixing of 0th and 1st diffraction orders within the detector integration window. Low SBR uses up the detector dynamic range and can reduce the spectral resolution further by increasing the noise level due to the detector limitations, which are not considered in this analysis.

The following sections explore two critical effects observed in Fig. 5 and Fig. 6; the cyclic nature of the interferogram that is observed in Fig. 4(c) and Fig. 4(d) and the decrease in the SBR in Fig. 5(b) and Fig. 5(d). Based on the results of this section, one can state that the spectral resolution can be kept < 15cm^{-1} which is close to the theoretical limit of 10cm^{-1} for a displacement of 500um.

4.2 Optimization results

Figure 7 illustrates the spectral resolution and SBR contours for a range of wavelength and grating period combinations assuming point source (θ_d = 0) and a finite size source with θ_d limited to 2.5°. The spectral resolution worsens at large wavelengths and small grating periods, where Talbot phase reversal distance is smaller than the mechanical displacement and interferograms with cyclic constrast variation are observed. Furthermore SBR is inversely proportional with the spectral resolution since SBR decreases due to Talbot phase reversals as well. The irregularities in the lower right parts of the figure are due to the large fluctuations in the width and the peak values of a multi-lobed spectrum [e.g. see Fig. 5(c) and Fig. 5(d)]. Those regions are not of interest due to poor resolution and low SBR performance.

When the divergence is introduced SBR decreases significantly for large diffraction gratings periods and the small wavelength regions due to order mixing at diffraction angles smaller than the divergence. Note that, when the incidence angle of the illuminating beam in the axis perpendicular to the grating fingers is not normal, strong shadowing effects would be observed that reduces both the SBR and the spectral resolution rapidly.

It is possible to avoid Talbot phase reversals by choosing the grating period sufficiently large. On the other hand, keeping the SBR high demand smaller grating periods for high dynamic range detection. The optimal grating period for this case study seem to be in the 80um-120um range. The final selection depends on the application and the importance of different parts of the spectrum.

#115556 - $15.00 USD Received 14 Aug 2009; revised 23 Oct 2009; accepted 1 Nov 2009; published 6 Nov 2009
(C) 2009 OSA

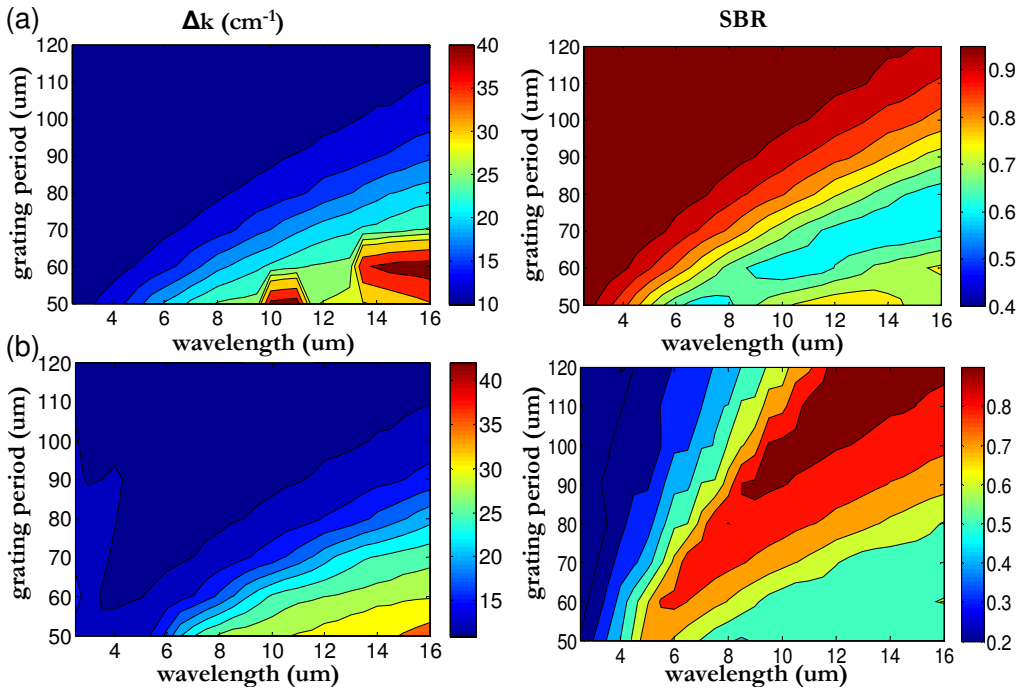


Fig. 7. Spectral resolution and signal to bias ratio contours for all wavelength and grating period range for a) $\theta_d = 0$ and b) $\theta_d = 2.5°$.

4.3 Analytical formulas

Undesired decrease in the fringe contrast created by the Talbot phase reversal can be modeled as illustrated in the interferogram of Fig. 8(a). For simplicity, the envelope of the interferogram is assumed to be a cosine function with a period of 2T. The divergence effect is not taken into account. The illustrated interferogram may be represented as:

$$I(x') = \left\{\left[0.5\cos\left(\pi x'/T\right)+0.5\right].\left[0.5\cos\left(2\pi x'/\lambda_0\right)\right]+0.5\right\} rect(x'/4d) \qquad (10)$$

where x′ is the OPD, which is twice the displacement x′ = 2x. The spectrum of the interferogram *S(k)* is the Fourier transform of Eq. (10). *S(k)* has a total of 7 dirac-delta terms. Those 3 terms of interest that are around the center wavenumber $k_o = 1/\lambda_o$ are given as below and illustrated in Fig. 8(b):

$$S(k)_{k\sim k_0} = \left[0.5\delta\left(k-\frac{1}{\lambda_0}\right)+0.25\delta\left(k+\frac{1}{2T}-\frac{1}{\lambda_0}\right)+0.25\delta\left(k-\frac{1}{2T}+\frac{1}{\lambda_0}\right)\right] * \mathrm{sinc}(4d(k)) \quad (11)$$

The spectrum exhibits multiple peaks around k_o, when Talbot period is small in compared to the displacement. This multi-peaking behavior was observed in Fig. 5(c) and Fig. 5(d).

From Eq. (11), the resolution can be expressed as

$$\Delta k = \frac{1}{T}+\frac{1}{2d} \qquad (12)$$

Equation (12) implies that the spectral resolution is a function of both the Talbot period and displacement. Furthermore, the spatial resolution converges to Eq. (1) for large Talbot periods. From Eq. (11) and Fig. 8(b), SBR can be calculated by summing the contribution of each peak at excitation wavelength, and can be expressed as:

#115556 - $15.00 USD Received 14 Aug 2009; revised 23 Oct 2009; accepted 1 Nov 2009; published 6 Nov 2009
(C) 2009 OSA

$$SBR = 0.5 + 0.5\mathrm{sinc}(2d / T) \quad (13)$$

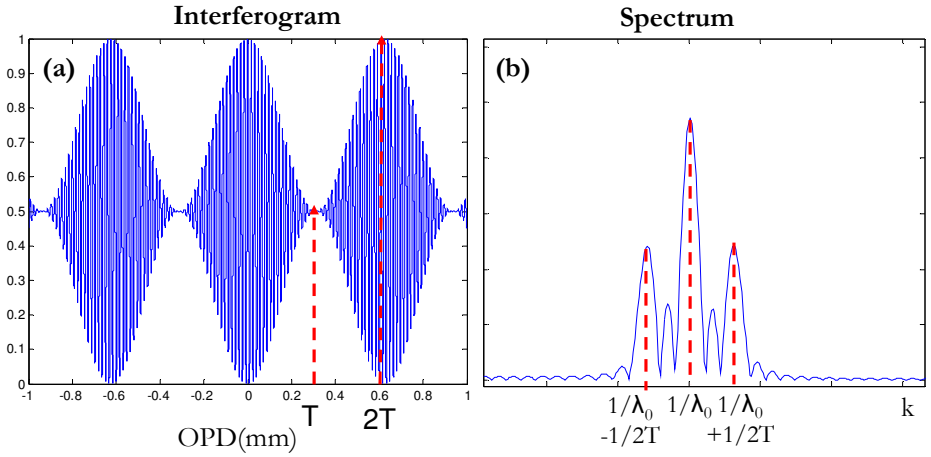


Fig. 8. a) An approximate interferogram corresponding to d, λ, and Λ combination. The interferogram envelope is obtained using Talbot phase reversal distance of T where fringe contrast vanishes. b) Corresponding spectrum

Figure 9 illustrates the Δk and SBR contours that are plotted using Eq. (12) and Eq. (13). The contours match quiet well with those in Fig. 7(a) for a divergence of 0 degrees. Using Fig. 7(a), Fig. 9, Eq. (12), and Eq. (13), one can conclude that Talbot phase reversal is the critical factor determining spectral resolution and SBR in an LGI spectrometer. Therefore, enforcing diffraction order separation as given by Eq. (5) is an over constraint in terms of achieving high spectral resolution and good SBR.

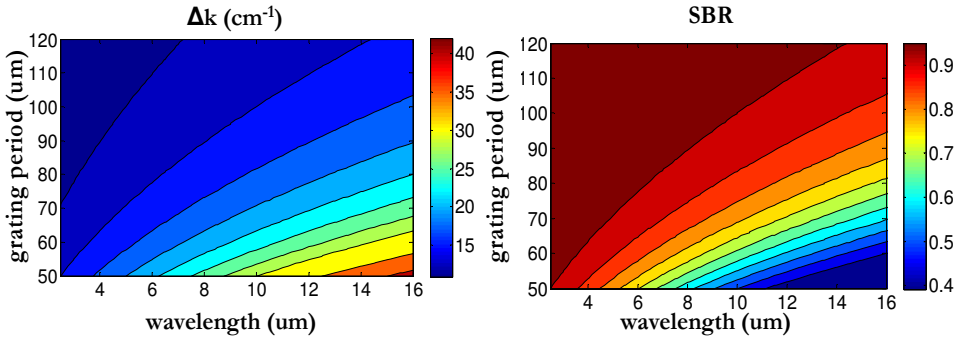


Fig. 9. spectral resolution and signal to bias ratio contours for all wavelength and grating period range, plotted using approximate analytical formulas given in Eq. (12) and Eq. (13).

5. Experimental results

Experiments were conducted using a red laser (λ = 633 nm), a diffraction grating etched into silicon with a period Λ = 40um in order to demonstrate the Talbot effect using a dynamic moving reflector placed underneath the grating. The moving platform is made using FR4 material and developed in our laboratory for FTS applications [7]. The distance of the FR4 platform to the grating was varied for 10 mm and the fringe contrast was recorded. Figure 10 illustrates the simulation and the experimental data of the interferogram envelope with respect to the distance between FR4 platform and the grating. Both simulated and experimental data agree perfectly with Talbot half period of $T/2$ = 2.5 mm. The experimental and simulation results are sensitive to incidence angle and the Talbot period changes rapidly if the incidence angle deviates from normal incidence in the direction perpendicular to the grating fingers.

#115556 - $15.00 USD Received 14 Aug 2009; revised 23 Oct 2009; accepted 1 Nov 2009; published 6 Nov 2009
(C) 2009 OSA

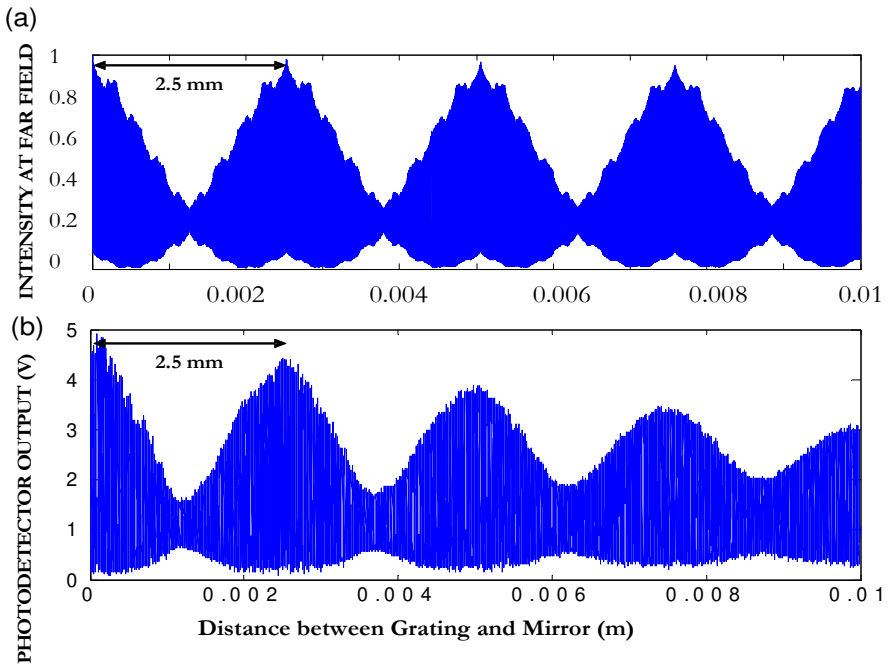


Fig. 10. (a) Interferogram obtained from simulation (b) Interferogram obtained from experiment

The experimental result is the first to report fringe contrast reduction based on Talbot phase reversals in a LGI based Fourier Transform Spectrometer. Previous large scale LGI spectrometers, having large grating periods and long phase reversal distances, do not exhibit this phenomenon [3,8,9]. The effect was not reported in recent MEMS based LGI spectrometers as well [4,10] due to relatively small mechanical displacements that is smaller than the Talbot period.

6. Conclusion

MEMS based LGI offers compact yet high resolution spectrometer architecture. The main limitation of LGI based spectrometer in contrary to Michelson configuration arises when the OPD is greater than the Talbot period. The Talbot limit was observed in both numerical simulations and in the experiments. For LGI based FTS systems, in order to achieve OPD limited spectral resolution, the grating period should be designed subject to the condition that $\Lambda>\sqrt{d\lambda}$ and the collimated beam divergence due to finite source size should be limited according to Eq. (4). Special attention to the incidence angle should be paid in the final setup in order to avoid further reductions in the Talbot period.

Furthermore, numerical results of Fig. 7 and approximate analytical formulas developed in Sec. 4(c) are useful to select a grating period for a given *d* and waveband in order to achieve the optimal spectral resolution and SBR.

The spectral resolution and SBR of LGI based FTS systems can be estimated fairly accurately using the equations Eq. (12) and Eq. (13).

Acknowledgment

This work is funded by MEMFIS 7th framework E.U project. We'd like to thank Arno Simon, Jean-Louis Stehle, Thilo Sandner and Michel Boyman for their help. O. F. and H. R. S acknowledge the support from TUBİTAK scholarship for graduate studies and H.U. acknowledges the support from TÜBA-GEBİP Distinguished Young Scientist award.

#115556 - $15.00 USD Received 14 Aug 2009; revised 23 Oct 2009; accepted 1 Nov 2009; published 6 Nov 2009
(C) 2009 OSA